



HAL
open science

Max-tree Computation on GPUs

Nicolas Blin, Edwin Carlinet, Florian Lemaitre, Lionel Lacassagne, Thierry
Géraud

► **To cite this version:**

Nicolas Blin, Edwin Carlinet, Florian Lemaitre, Lionel Lacassagne, Thierry Géraud. Max-tree Computation on GPUs. 2022. hal-03556296v2

HAL Id: hal-03556296

<https://hal.science/hal-03556296v2>

Preprint submitted on 8 Mar 2022

HAL is a multi-disciplinary open access archive for the deposit and dissemination of scientific research documents, whether they are published or not. The documents may come from teaching and research institutions in France or abroad, or from public or private research centers.

L'archive ouverte pluridisciplinaire **HAL**, est destinée au dépôt et à la diffusion de documents scientifiques de niveau recherche, publiés ou non, émanant des établissements d'enseignement et de recherche français ou étrangers, des laboratoires publics ou privés.

Max-tree Computation on GPUs

Nicolas Blin, Edwin Carlinet, Florian Lemaitre, Lionel Lacassagne, Thierry Géraud *Member, IEEE*

Abstract—In Mathematical Morphology, the max-tree is a region-based representation that encodes the inclusion relationship of the threshold sets of an image. This tree has proved useful in numerous image processing applications. For the last decade, work has led to improving the construction time of this structure; mixing algorithmic optimizations, parallel and distributed computing. Nevertheless, there is still no algorithm that benefits from the computing power of the massively parallel architectures. In this work, we propose the first GPU algorithm to compute the max-tree. The proposed approach leads to significant speed-ups, and is up to one order of magnitude faster than the current State-of-the-Art parallel CPU algorithms. This work paves the way for a max-tree integration in image processing GPU pipelines and real-time image processing based on Mathematical Morphology. It is also a foundation for porting other image representations from Mathematical Morphology on GPUs.

Index Terms—Mathematical morphology, hierarchical image representation, component-trees, max-tree, graph algorithms.

1 INTRODUCTION

ORIGINALLY from the mathematical morphology field, component trees are powerful and versatile structures that organize the level sets of an image as tree. The min- and max-trees were first introduced in [2], motivated by the gain in interest for connected operators. Connected filters preserve the contours of the objects of an image by merging only its flat zones. These operators have been known for quite a long time and date back to the 90s [3], [4], but they are still widely used in today's image processing pipelines for efficient pre- or post-processing steps (e.g., background removal for brain lesion detection [5], noise removal [6]).

Connected filters are directly linked to the min- and max-trees as these structures enable simple and efficient implementations of such filters [7]. These trees facilitate the development of more advanced forms of filtering: based on attributes [8], [9], with non-trivial filtering rules [10], or with new generation connectivities [11]. Some uses of the max-tree are illustrated in figure 1.

Beyond filtering and image processing, component trees are used in computer vision-related tasks. For instance, pattern spectra and attribute profiles, that compute the distribution of sizes and shapes of image regions, have been used with success in classification of satellite and astronomical images [12], [13], [14] and content-based image retrieval [15], [16]. Maximal Stable Extremal Regions [17] are well-known descriptors used to find correspondences between images and fast linear algorithms are based on the max-tree [18]. Region-based analysis using morphological trees have also been used in medical imaging, e.g., for blood vessel segmentation [19] and 3D visualization [20].

Min- and max-trees are also at the basis of other image representations. In [21], a self-dual hierarchical representation, the tree of shapes (ToS), encodes the inclusion of the

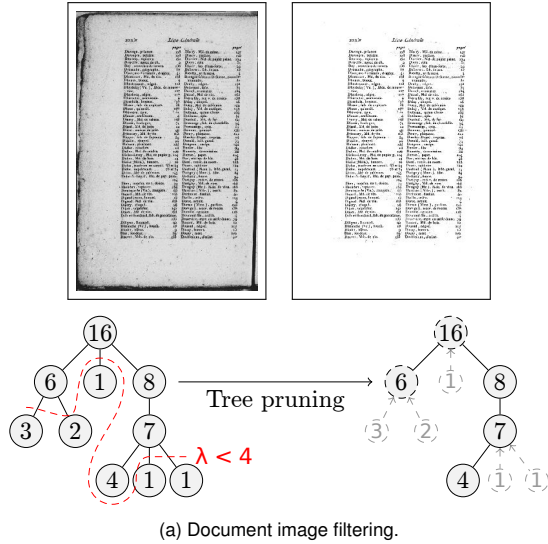
level lines. It is computed by merging the min- and max-trees. Later, [22] propose a ToS construction pipeline where the last stage consists of a max-tree computation.

When it comes to deploying image processing methods, fast algorithms are required. This might be due to some real-time constraints, or because the amount of data to process is increasing steadily. A typical pipeline using the max-tree has three steps: construction of the max-tree, attribute computation and filtering, and image restitution. However, more than 90% of the pipeline duration is spent in the construction of the tree [23]. Many algorithms have been developed for speeding-up the max-tree computation. So far, the proposed optimization techniques can *roughly* come under one of these three categories: (a) algorithmic optimizations, i.e., choosing between a top-down or a bottom-up construction with adapted data structures [18], [24], [25]; (b) thread level parallelism, i.e., classical parallelism for multiprocessors with shared memory (SMP) [26], [27], [28]; (c) distributed computing, i.e., joint max-tree computation between distributed memory [29], [30]. To the best of our knowledge, **this is the first time a max-tree algorithm is proposed for massively parallel architectures and fits the SIMT paradigm of GPUs.**

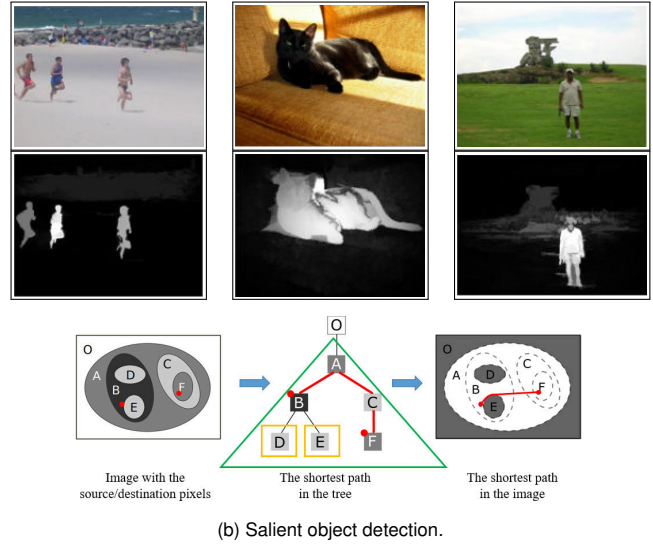
The paper is organized as follows. In section 2, we recall the definition of the max-tree and in section 3, we provide an overview of the sequential, parallel and distributed State-of-the-Art max-tree computation algorithms. We also make some links with the Connected Component Labeling algorithms, in particular those dedicated to GPUs as they will be the base of our proposal. In section 4, we depict our proposed max-tree algorithm with implementation details for hierarchical memory models. In section 5, we propose some optimized version taking advantages of the super-efficient max-tree algorithm for 1D-signals, and extra optimizations to handle the 8-connected grid and high-quantized images. In section 6, we compare the performance of our algorithms to the State-of-the-Art sequential and parallel ones on three ranges of architectures (desktop stations, mobile devices and servers). Last, we give perspectives in section 7 and conclude in section 8.

- Nicolas Blin, Edwin Carlinet, and Thierry Géraud are with EPITA Research and Development Laboratory (LRDE), Paris, France. (Contact: firstname.lastname@lrde.epita.fr)
- Florian Lemaitre and Lionel Lacassagne are with LIP6, ALSOC team, Sorbonne University, CNRS, Paris, France. (Contact: firstname.lastname@lip6.fr)

Manuscript received April 19, 2005; revised August 26, 2015.



(a) Document image filtering.



(b) Salient object detection.

Fig. 1: Image processing with the max-tree. (a) Background extraction for document image analysis with a morphological black top-hat. The min-tree is pruned by removing connected small peak components (< 4 pixels that do not touch the border). The residue (filtered components) forms the clean text and the background is removed. (b) Salient object detection for scene analysis [1]. A morphological tree is used to compute the Dahu distance from image borders. This distance that mixes geodesic distance and gray-level distances can be computed using a tree similar to the max-tree (the tree of shapes).

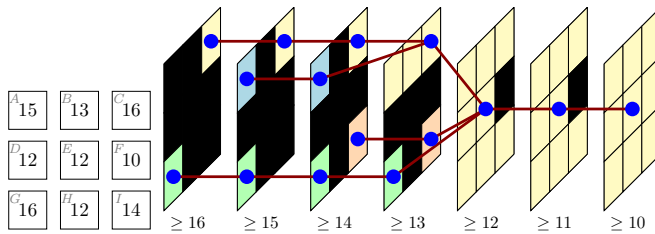


Fig. 2: Level set decomposition of an image and its max-tree. The connected components of $[f \geq \lambda]$ are included in those from $[f \geq \lambda - 1]$ and form an inclusion tree.

2 FOREWORDS

2.1 Mathematical preliminaries

Let $f : \mathbb{Z}^2 \rightarrow \mathbb{N}$ be a 2D regular image of N pixels having values on a totally ordered set of G grayscale levels. Let \mathcal{N} be a neighborhood on the 2D grid (typically the 4- or 8-connectivity). Given a set of points X , we note $CC(X) \subset \mathcal{P}(\mathbb{Z}^2)$ the set of the connected components of X given the neighborhood \mathcal{N} .

Let $\lambda \in \mathbb{N}$ be a gray level, $[f \geq \lambda]$ is the *upper level set* of f at level λ and $CC([f \geq \lambda])$ are the *upper components*. The *upper peak component* of a pixel x at level λ noted P_x^λ is the upper component $U \in CC([f \geq \lambda])$ such that $x \in U$. When λ is omitted as in P_x , λ is implicitly $f(x)$, and P_x is said to be the *upper level component* of x .

The family $\{CC([f \geq \lambda])\}_\lambda$ is increasing, each element of $CC([f \geq \lambda + 1])$ being included in those of $CC([f \geq \lambda])$, this family can be represented with an inclusion tree called the max-tree as shown in figure 2.

2.2 Max-tree representation

Max-trees can be represented in a compact way using the representation from [24]. A node of the max-tree represents a peak component and the edges stand for the inclusion of

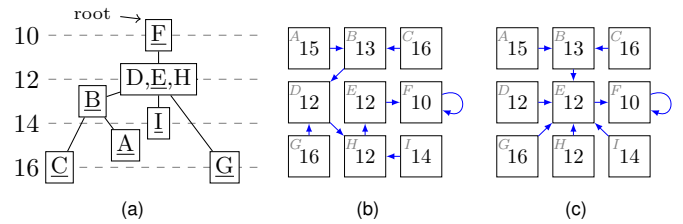


Fig. 3: *parent* image encoding the max-tree of figure 2. (a) is the max-tree to encode, some pixels appear underlined as they are randomly chosen to be the canonical elements. The *parent* relation appears in blue in (b). (b) is not path-compressed as some pixels point to non-canonical elements. (c) is the result of the canonicalization of (b).

these components. A node stores only the pixels that are not already part of some “sub”-nodes. In figure 3-a, the node at level 13 represents the component $\{A, B, C\}$ but only stores the pixel B (A and C already belong to some other nodes). This encoding enables one pixel to be associated to exactly one max-tree node. Then, an image *parent* is used to store the *inclusion* relationship between nodes (figure 3-b). For that purpose, a node is represented by only one of its pixels, the so-called *canonical* element. Every other pixel that belongs to the node is *linked* to the canonical element (directly or indirectly by other non-canonical elements of the node). A tree is said *canonical* if every path is compressed, i.e., if every pixel directly links to a canonical element. *Canonicalization* consists in following the *parent* path from each pixel to the first canonical element and replacing it by a direct edge (figure 3-c). The *parent* image in figure 3-b is not canonical, because some pixels (namely B, D, G, I) do not point to canonical elements. Since the canonical elements are arbitrarily chosen, there may exist several valid *parent* images. To ensure the uniqueness of the representation, we need a total ordering between pixels, e.g. the scanning order, that designates the bottom-right most pixel as the canonical element of the component. More formally, let \prec be the total

order between pixel:

$$p < q \Leftrightarrow f(p) < f(q) \text{ or } (f(p) = f(q) \text{ and } p > q)$$

A special point *null* is used as the root's parent and verifies $\forall p, null < p$ (it is the infimum over $<$). The parent image should also meet the following two conditions. (a) $\forall p, parent(p) < p$, and (b) $\forall p, parent(p)$ is canonical (the tree is canonicalized)

3 STATE-OF-THE-ART

3.1 Sequential Max-tree algorithms

Immersion-based algorithms [24], [25] are based on the Tarjan's Union-Find (UF) [31] algorithm that builds the tree from leaves to root. These algorithms start by sorting the pixels of the image w.r.t. their grayscale level. Disjoint sets are created for each pixel, and are merged in increasing order according to their gray level. The process is similar to the Union-find based connected component labeling algorithms where each connected set is encoded as a tree, but it adds a constraint on the merge order. The algorithm is sketched on algorithm 1. It relies on three operations that update the disjoint trees:

- MAKE-SET(parent, x) creates the singleton set $\{x\}$. It basically sets $parent(p) \leftarrow null$
- FIND-ROOT(parent, x) follows the chain of *parent* up to the root.
- UNION(parent, x, y) merge *x*'s and *y*'s trees and set *x* as the new root.

Union-find based algorithms have a quasi-linear complexity, provided that: (a) the pixels can be sorted in linear time (e.g., using radix-sort); (b) FIND-ROOT implements the path-compression technique that updates the parent pointer of all the nodes of the chain (it also implies having two separate structures, one encoding the compressed tree and another one encoding the real max-tree); (c) UNION uses the union-by-rank technique and chooses the new root so that the tree remains balanced. Once the tree has been constructed, the FLATTEN procedure in algorithm 1 is responsible for canonicalizing the tree. The nodes are traversed from root to leaves to propagate the *canonical* property. Indeed, at line 4, $parent(q)$ is ensured to be a representative node.

Flood-based algorithms [2], [18], [32], [33] proceed in the opposite way and build the tree from root to leaves. They start from a point (generally the root, i.e. the global minimum) and flood the peak component located at this point with a depth-first traversal graph pattern. The pixels at the border of this peak component are queued in a priority queue for later processing. Once the peak-component is flooded, a local subtree has actually been built and is then attached to the parent node. Then, the process continues in a recursive way with the point at highest priority in the queue. The process ends when the whole image is flooded. Flood-based algorithms are generally faster than their union-find based counterparts, especially for low-dynamic range images [34] where stacks and hierarchical queues are used to remove the recursion and efficiently implement the processing queue.

Algorithm 1 Scheme of a union-find-based max-tree algorithm.

```

1: procedure MAXTREE(f)
2:   S ← sort (<) pixels increasing
3:   for all p do parent(p) ← undef
4:   for p in S backward do
5:     MAKE-SET(parent, p)
6:     for n in N(p) do
7:       if parent(n) ≠ undef then
8:         r ← FIND-ROOT(parent, n)
9:         if r ≠ p then UNION(parent, p, r)

1: procedure FLATTEN(f)
2:   for p in S forward do
3:     q ← parent(p)
4:     if q is not null and f(parent(q)) == f(q) then
5:       parent(p) ← parent(q)

```

Algorithm 2 1D-Maxtree algorithm.

```

1: function UNSTACK(f, r, lvl)
2:   while !StackEmpty() and lvl ≤ f(StackTop()) do
3:     parent(r) ← StackPop()
4:     r ← parent(r)
5:   return r

5: procedure 1D-MAXTREE(f, parent)
6:   r ← start_index
7:   for all p starting at start_index + 1 do
8:     if f(r) < f(p) then
9:       StackPush(r)
10:      r ← p
11:    else if f(r) = f(p) then parent(p) ← r
12:    else
13:      r ← UNSTACK(f, r, f(p))
14:      if f(r) > f(p) then
15:        parent(r) ← p
16:        r ← p
17:      else parent(p) ← r
18:   r ← UNSTACK(f, r, -∞)
19:   parent(r) ← null

```

1D-Maxtree algorithm [35] is a linear algorithm (algorithm 2) dedicated to the max-tree computation of 1D-signals. It is single pass and very memory efficient as it only requires a constant-size stack (actually $O(\min(G, N))$).

The algorithm iterates over the 1D image starting at *start_index* and acts based on the gray level difference between the current and last pixel (*p* and *r* respectively). Three cases can arise as depicted in figure 4. If the gray level increases ($f(r) < f(p)$), last pixel is pushed into the stack, creating a new connected component. If the gray level stays the same ($f(r) = f(p)$), the current connected component

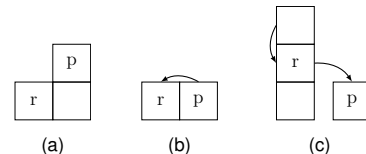


Fig. 4: Three possible cases during the 1D algorithm

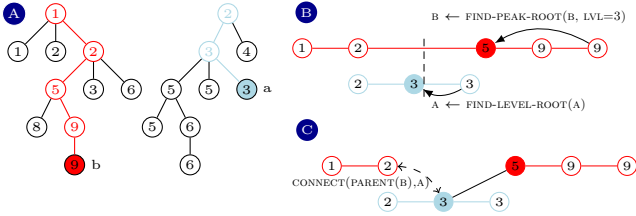


Fig. 5: Merging max-trees. (A) Two disjoint trees to merge by linking a and b . (B) The corresponding branches are followed until the nodes to merge are found. (C) The parent pointer of b is updated, and the connection is made recursively with the old parent.

Algorithm 3 Algorithm used to merge two max-trees.

```

1: function FIND-PEAK-ROOT( $parent, x, lvl$ )
2:    $q \leftarrow parent(x)$ 
3:   while  $q$  not null and  $lvl \leq f(q)$  do
4:      $x \leftarrow EXCHANGE^1(q, parent(q))$ 
5:   return  $x, q$ 

1: function FIND-LEVEL-ROOT( $parent, x$ )
2:   return FIND-PEAK-ROOT( $parent, x, f(x)$ )

1: procedure CONNECT( $a, b$ )
2:   while  $b$  not null do
3:     if  $f(b) < f(a)$  then SWAP( $a, b$ )
4:      $a, \_ \leftarrow FIND-LEVEL-ROOT(parent, a)$ 
5:      $b, \_ \leftarrow FIND-PEAK-ROOT(parent, b, f(a))$ 
6:     if  $b \prec a$  then SWAP( $a, b$ )
7:     if  $a = b$  then return
8:      $b \leftarrow EXCHANGE(parent(b), a)$  ▷ merge-set

```

is extended. The last case, when the gray level decreases, is divided into three scenarios: If the stack is empty, no intermediate component exists between p and r , thus p directly becomes r parent's. If the stack is not empty, the parent of p might be in the stack. The UNSTACK() function pops the stack as long as the levels are greater than the current level, linking components in the stack along the way. If a lower gray level is found at the top, p is the intermediate component between the last and current stack top thus r becomes parent of p . Else, the stack has been emptied, there is no intermediate component (and thus $f(r) > f(p)$), p can be set as parent of r . Finally, if there are elements left in the stack we can directly link them together using UNSTACK() and set the last element as the root of the tree.

3.2 Parallel and distributed max-tree algorithms

Merge-based algorithms rely on a divide-and-conquer strategy to compute the max-tree. The image is split into tiles for which local max-trees are computed. Then, the local max-trees are merged hierarchically with a reduction pattern by connecting the pixels on the tile boundaries. Figure 5 illustrates the merge of two max-trees that have to be connected through the edge (a, b) . The corresponding algorithm is given in algorithm 3. First, FIND-PEAK-ROOT follows up the chains of a and b to reach the nodes that have to be updated. Supposing $f(a) < f(b)$, it requires reaching the level-root of a (because it may not be the canonical element),

1. $x \leftarrow EXCHANGE(p, q) := old \leftarrow p; p \leftarrow q; x \leftarrow old;$

and then, reaching the root of the peak component $P_b^f(a)$ (i.e., the highest node with level not greater than $f(a)$). The procedure returns the canonical node and its parent (which is not used for now). If nodes have both the same level, the merge applies on flat-zones, we need to select the "smallest" representative in terms of \prec to be the new root. The parent of b is updated and CONNECT is called recursively on the parent until reaching the root.

This process is well-adapted to the parallel construction of the max-tree because each tile computation is independent. The first parallel algorithms [26], [27], [28] were using this algorithm on shared-memory systems with scalable results (almost linear in the number of threads). As images grew in size, the same strategies were adopted for a distributed computation of the max-tree [29], [36] with the extra burden of minimizing memory exchanges between (cluster) nodes using border max-trees. This idea is even pushed further in [30], [37] with a distributed max-tree representation based on border max-trees that avoids storing the final tree in shared-memory and enables distributed tree processing.

3.3 Connected Component Labeling on GPU

As Max-Tree computation is close to Connected Component Labeling (CCL), it is interesting to look at the State-of-the-Art for CCL algorithms. The first algorithms for CCL on GPU date back to the late 00s [38] and were repeating a label propagation until stability. However, they have been superseded in image processing by concurrent algorithms based on the Union-find (UF) structure to compute the equivalences between pixels.

Concurrent Union-Find is an old problem [39], [40], but until recently, it was not used for CCL. The first CCL implementation on GPU came in 2015 from Komura [41] using a concurrent Union-Find. The paper also introduces the Komura Equivalence (KE) that modifies the initialization step of the UF to resolve some equivalences on-the-fly and avoids the creation of temporary single-node equivalence trees. In 2018, the Playne algorithm [42] improves upon KE by analyzing pixel patterns in order to avoid redundant merge operations. In 2018, the HA algorithm [43] sped up the Playne algorithm by using small segments (32-pixel wide, the warp size) of pixels and CUDA intrinsics. Later, in 2019, the BKE algorithm [44] (Block-based Komura Equivalence) improves the Playne algorithm by exploiting a property of 8-connected components to process pixels in 2×2 blocks. In 2021, the Full-Length Segment Labeling is able to tackle segment longer than the warp size, and advanced algorithmic optimizations reduce the voting bottleneck of Connected Component Analysis algorithms [45].

The concurrent Union-Find consists in retrying to link two roots in a CAS-loop. If the higher root is updated by another thread, the link is retried with the new parent of the formerly higher root. This algorithm is in fact wait-free as the work of a thread is bounded by the height of the resulting tree. It is detailed in algorithm 4. While the original concurrent Union-Find was using a CAS for the retry, [41] used an ATOMICMIN to leverage the natural ordering of labels and reduce the practical number of retries.

Figure 6 is a timeline example that demonstrates how multiple threads can concurrently modify the Union-Find structure. It also shows the difference between the

Algorithm 4 Concurrent Union-Find on GPU for Connected Component Labeling.

```

1: procedure FIND-ROOT( $L, a$ )
2:   while  $a \neq L[a]$  do
3:      $a \leftarrow L[a]$ 
4:   return  $a$ 
1: procedure UNION( $L, a, b$ )
2:    $a \leftarrow$  FIND-ROOT( $L, a$ )
3:    $b \leftarrow$  FIND-ROOT( $L, b$ )
4:   while  $a \neq b$  do
5:     if  $b < a$  then SWAP( $a, b$ )
6:      $c \leftarrow$  ATOMICMIN( $L[b], a$ )
7:     if  $c = b$  then return
8:      $b \leftarrow c$ 
    
```

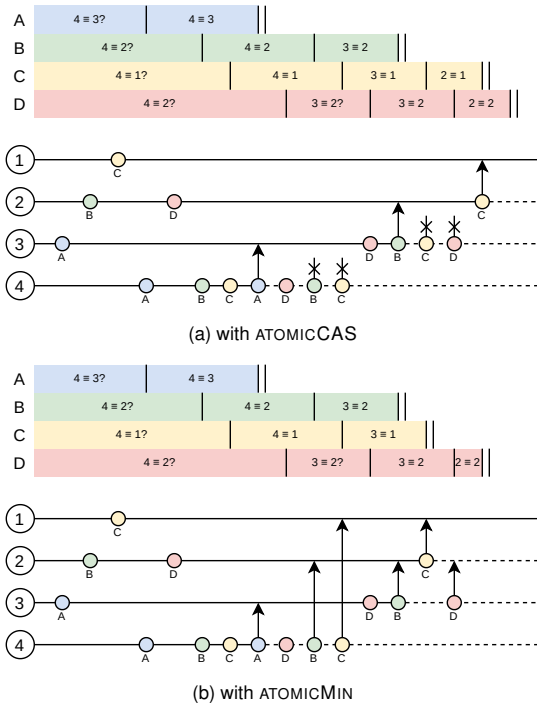


Fig. 6: Example of a lock-free Union-Find. Four threads (A, B, C and D) process the following unions: $4 \equiv 3$, $4 \equiv 2$, $4 \equiv 1$ and $4 \equiv 2$. The schemas are a timeline of the states of each thread and the operations in memory. A circle corresponds to a *read*, while an arrow corresponds to a *write*, the end of the arrow being the value written. An arrow with a circle is a read-modify-write atomic, and the cross stands for a failure (only for CAS). The solid lines for labels represent root labels, while dashed ones correspond to labels whose parent have been set. For the sake of demonstration, threads follow a round-robin scheduling.

ATOMICCAS-based function and the ATOMICMIN-based one (respectively figure 6a and figure 6b). We can clearly see that the ATOMICMIN version have one less read-modify-write atomic, and that the final tree is flatter (label 4 points to label 1 directly).

4 A MAX-TREE ALGORITHM FOR GPUS

4.1 Sort-less max-tree algorithm

The first step of algorithm 1 consists in sorting the pixels so that merging the disjoints subtrees with the union-find occur from the leaves to the root of the max-tree. Using the

Algorithm 5 Sort-less max-tree algorithm.

```

1: procedure MAXTREE( $f$ )
2:   for all pair of neighbors ( $p, q$ ) do
3:     CONNECT( $p, q$ )
1: procedure FLATTEN( $f$ )
2:   for all  $p$  do
3:      $q \leftarrow$  parent( $p$ )
4:     parent( $p$ )  $\leftarrow$  FIND-LEVEL-ROOT(parent,  $q$ )
    
```

Algorithm 6 Concurrent lock-free version of algorithm 3

```

1: procedure CONNECT( $a, b$ )
2:   while  $b$  not null do
3:     if  $f(b) < f(a)$  then SWAP( $a, b$ )
4:      $a, _ \leftarrow$  FIND-LEVEL-ROOT(parent,  $a$ )
5:      $b, _ \leftarrow$  FIND-PEAK-ROOT(parent,  $b, f(a)$ )
6:     if  $b < a$  then SWAP( $a, b$ )
7:     if  $a = b$  then return
8:      $b \leftarrow$  ATOMICMAX $\prec$ (parent( $b$ ),  $a$ )
    
```

parallel strategies depicted in section 3.2, we can actually build a max-tree using only tree merges. It consists in calling CONNECT for every edge in the image as shown in algorithm 5. The complexity of this algorithm is $O(G \cdot N)$ and thus highly depends on the number of levels G .

4.2 Concurrent computation of the max-tree

As it stands, the current algorithm cannot be run concurrently as there may be data races when updating the *parent* pointer in algorithm 3 in line 8. Even if read and write operations were atomic, an update might not be seen by the other threads (lost-update problem). The solution lies in the same technique used for the concurrent labeling algorithm exposed in section 3.3. A read-modify-write operation is used when updating the parent pointer. The situation is a bit more complex as we need to select the right node if a conflict occurs. In algorithm 4, ATOMICMIN is used because the representative is chosen to be the lowest label. Choosing the minimum (or the maximum) prevents the creation of cycle that could occur with concurrent updates.

With the max-tree, the same problem arises if there is no total order imposed on pixels. In algorithm 6, line 8 uses ATOMICMAX based on \prec to select the right parent when concurrent updates occur. Suppose that the parent of a node has to be updated concurrently with q_1, q_2 and q_3 . The new root will be the "lowest" one (i.e., the one with the highest level). If there are several "lowest" nodes, we then need to select the right representative which is the most bottom-right node. In case of conflict, two cases occur:

- The ATOMICMAX updates the value and makes progress. In this case, the old value of *parent*(b) is held in b , we need to merge the old parent node with a .
- The ATOMICMAX does not update the value and fails to make progress. *parent*(b) has been updated by another thread and is stored in b . We still have $a < b$ (otherwise it would have succeeded), thus it retries to connect the updated parent (b) with a .

Algorithm 6 uses an ATOMICMAX based on a non-trivial relation that involves comparing gray levels and pixel in-

Algorithm 7 Concurrent lock-free CONNECT with a CAS

```

1: procedure CONNECT(a,b)
2:   while b not null do
3:     if f(b) < f(a) then SWAP(a, b)
4:     a, A ← FIND-LEVEL-ROOT(parent, a)
5:     b, B ← FIND-PEAK-ROOT(parent, b, f(a))
6:     if b < a then SWAP(a, b) SWAP(A, B)
7:     if a = b then return
8:     old ← ATOMICCAS(parent(b), B, a)    ▷ Try
9:     if old = B then                    ▷ If false → retry
10:    b ← old
    
```

dexes, but most GPUs support atomic operation on trivial types only. To overcome this limitation, the parent image is used to store 32-bit records such that comparing the records with $<$ is equivalent to comparing the binary representation of the record. Using the LSB 0 bit numbering, $parent(x)$ stores in 32 bits:

x 's current level	x 's parent level	x 's parent index
32	24	16
		0

Supposing the pixel are 1-based indexed, the *null* value is thus encoded with 0 (0 for all fields). In algorithm 6, line 8 becomes:

```

8: newB ← [f(b), f(a), a]
9: [_, _, b] ← ATOMICMAX(parent(b), (uint32_t)newB)
    
```

When $parent(x)$ is updated, the *current level* always remains the same, but the *parent level* and the *parent index* might be updated by this new parent if they are greater than the original ones.

This representation works for images with at most $2^{16} - 1$ pixels because the parent index is 1-based and encoded in 16 bits. To handle 32-bit indexes, this representation can be extended to 64 bits at the cost of doubling the shared memory usage. Alternatively, an ATOMICCAS (see algorithm 7) can be used instead of this representation but leads to more *retries*. Indeed, in case of conflicts, only one thread makes progress with a CAS; while using an ATOMICMAX, several threads may update the same parent in the same turn.

4.3 Concurrent max-tree computation pipeline

The algorithm has been adapted to fit the hierarchical memory model of CUDA and minimize global memory loads and stores. It has three main parts depicted in figure 7.

Local max-tree construction. The image is tiled into blocks with as many threads as pixels in the block. (a) All the threads start with loading the input image values into the field *current level* of the *parent* image in shared memory; – the size of the block is small enough for using 16-bit local indexes – (b) CONNECT is called for every pair of neighbors (twice per thread if using the 4-connectivity) as shown in figure 7b; (c) the *parent* image is flattened to make the local max-tree canonical; (d) the *parent* image block is copied from shared memory to global memory, converting local indexes to 32-bit global indexes.

Global max-tree merging (figure 7c). The local max-trees have to be merged along the block boundaries. With

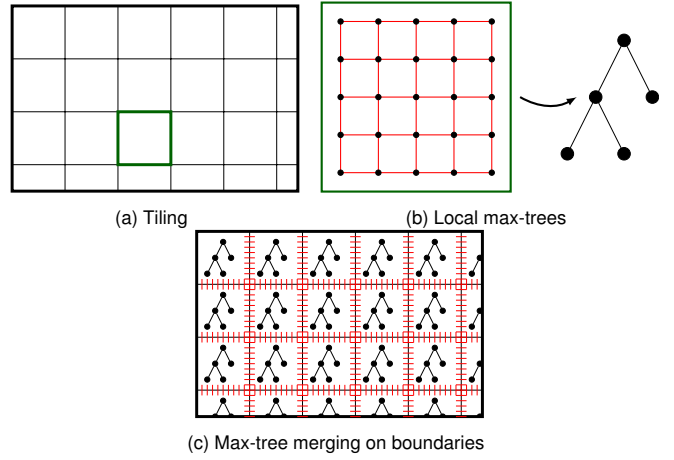


Fig. 7: Hierarchical computation of the max-tree. (a-b) Local max-trees are first computed on tiles by thread blocks in shared memory and then merged in global memory (c). Each red edge leads to concurrent calls to CONNECT with the corresponding endpoints.

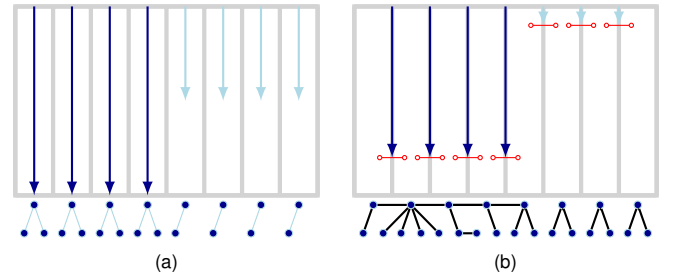


Fig. 8: 1D-optimized max-tree building. Two thread warps first build the column max-trees (a) then merge concurrently by iteratively calling CONNECT on the both side of the boundaries (b).

as many threads as the number of pixel pairs on the block boundaries, CONNECT is called with the pair of pixels along vertical and horizontal boundaries. The merge acts on global memory with 32-bit indexes (so using algorithm 6).

Flattening. The *parent* image is tiled into blocks and each block is flattened.

5 ALGORITHMIC VARIATIONS

5.1 Optimized local max-tree

As depicted in section 4.1, to build a max-tree on GPU, one could just call the concurrent CONNECT for every edge in the image. This has the drawback of generating many concurrent writes which hurts performance [45] even when issued in shared memory. To reduce the number of calls to CONNECT, local max-trees are first built column-wise using the 1D algorithm depicted in algorithm 2 (see figure 8-a). This algorithm is inherently fast because there are no data dependencies between threads. Inside each tile, each thread inside each thread block starts by fetching the first pixel of its column i.e. the first line of the tile. As each thread unravels its execution path, the thread block keeps on fetching, in a coalesced manner, the lines of the tile. Since each thread is working on its own column max-tree, no atomic nor syncing operations are required. There are also no bank-conflict as each thread works on its own bank.

Once local max-trees are built inside the tile, each thread (besides the last one) sweeps again top to bottom, calling

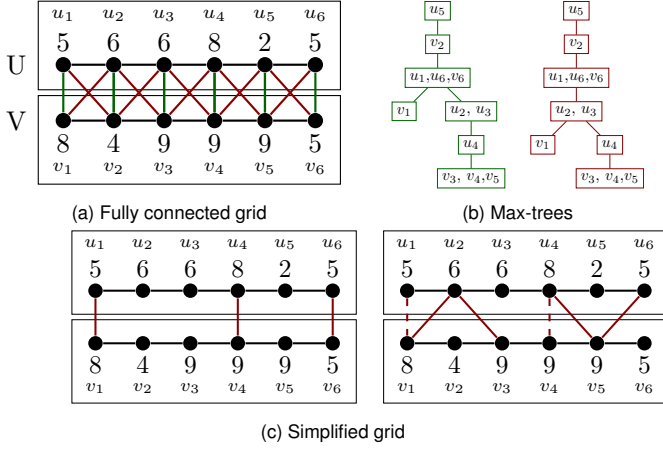


Fig. 9: Connecting columns and tile boundaries. The 4-connected and 8-connected neighborhood (a) and the corresponding max-trees in 4-connectivity (b-left) and 8-connectivity (b-right). The simplified connectivity grids for 4-connectivity (c-left) and 8-connectivity (c-right) give the same max-trees.

the concurrent CONNECT on each of the remaining edges (figure 8-b). This effectively cuts by half the number of CONNECT needed and significantly improves performance.

5.2 Grid simplification for 8-connection

The extension to 8-connectivity is straightforward. When merging columns or tiles, one just needs to call CONNECT in the diagonal directions (see figure 9a). It follows that the number of CONNECT calls doubles during the local construction of the *Base* algorithm and triples when merging columns or at tile boundaries. This is experimentally confirmed in section 6.2, showing that the processing time of the *base* algorithm increases by 120% on average, while the time of the *1D-optimized* algorithm is multiplied by a factor 2.5. Again, it confirms that CONNECT is an expensive operation, and we should minimize its use.

Let f be an image with two disjoint rectangular regions that connect over the boundary pixels $U = \{u_1, u_2, \dots, u_n\}$ and $V = \{v_1, v_2, \dots, v_k\}$. Let E be the set of edges that connects U to V . Considering the 4-connected grid G_4 , $E = \bigcup_{1 \leq k \leq n} E_k$ where $E_k = \{(u_k, v_k)\}$, i.e, there are n calls to CONNECT. With the 8-connected grid G_8 , $E_k = \{(u_k, v_k), (u_{k-1}, v_k), (u_k, v_{k-1})\}$ (for $k > 1$), so there are three calls to CONNECT for each k . To reduce the number of calls to CONNECT, we rely on the following propositions.

Proposition 1. *Considering the 8-connectivity, the max-tree of f with edges E is equivalent to the max-tree of f with the set of edges $E' = \cup E'_k$ where $E'_1 = E_1$ and for $k > 1$:*

$$E'_k = \begin{cases} \{(u_k, v_k)\} & \text{if } f(u_k) > f(u_{k-1}) \wedge f(v_k) > f(v_{k-1}) \\ \{(u_{k-1}, v_k)\} & \text{if } f(u_k) \leq f(u_{k-1}) \wedge f(v_k) > f(v_{k-1}) \\ \{(u_k, v_{k-1})\} & \text{if } f(u_k) > f(u_{k-1}) \wedge f(v_k) \leq f(v_{k-1}) \\ \emptyset & \text{otherwise} \end{cases}$$

Proof. It is worth mentioning that an edge (u, v) is only involved in the construction of P_u^α and P_v^α with $\alpha \leq \min(f(u), f(v))$. Let $k \in \mathbb{N}$, $1 \leq k \leq n$ and

$$\begin{aligned} (a, A) &= (u_k, u_{k-1}) \text{ if } f(u_k) < f(u_{k-1}) \text{ else } (u_{k-1}, u_k) \\ (b, B) &= (v_k, v_{k-1}) \text{ if } f(v_k) < f(v_{k-1}) \text{ else } (v_{k-1}, v_k) \end{aligned}$$

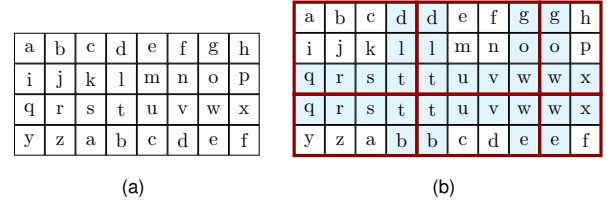


Fig. 10: Tile border duplication with tiles of size 4×3 . (a) Original image (b) Image with halo. Note that small tiles are used for illustration purposes, but the ratio of duplicated pixels is actually much lower in real cases.

Then (a, b) , (a, B) and (A, b) are useless edges in the max-tree construction as they do not change the peak components.

Let $\alpha = \min(f(a), f(b))$. a and b connects through the path $a \leftrightarrow A \leftrightarrow B \leftrightarrow b$, with $\min(f(A), f(B), f(a), f(b)) \geq \alpha$, so $P_a^\alpha = P_b^\alpha$ with or without (a, b) .

Let $\alpha = \min(f(a), f(B))$. a and B connects through the path $a \leftrightarrow A \leftrightarrow B$ with $\min(f(A), f(B)) \geq \alpha$, so $P_a^\alpha = P_B^\alpha$ with or without (a, B) .

Let $\alpha = \min(A, b)$. A and b connects through the path $A \leftrightarrow B \leftrightarrow b$ with $\min(f(A), f(B), f(b)) \geq \alpha$, so $P_A^\alpha = P_b^\alpha$ with or without (A, b) .

By recursively removing the useless edges for all k (in whichever order), proposition 1 holds. Note that the edge (u_{k-1}, v_{k-1}) might be missing for some k . Nevertheless, the equivalence holds as there still exists an equivalent path. \square

Proposition 2. *Considering the 8-connectivity, the max-tree of f with edges E' is equivalent to the max-tree of f with the set of edges $E'' = \cup E''_k$ where $E''_n = E'_n$ and for $k < n$:*

$$E''_k = \begin{cases} E'_k \setminus \{(u_k, v_k)\} & \text{if } f(u_k) < f(u_{k+1}) \vee f(v_k) < f(v_{k+1}) \\ E'_k & \text{otherwise} \end{cases}$$

Proof. Similar to the previous proof. There exists an alternative path that do not pass by (u_k, v_k) . \square

From proposition 1 and proposition 2, it follows that $|E''_k| \leq 1$. In the context of the merging tile boundaries, it follows that **there is at most one CONNECT per thread**. The grid simplification can also be applied with the 4-connected grid using proposition 3 which also makes it possible to remove some unnecessary calls to CONNECT.

Proposition 3. *Considering the 4-connectivity, the max-tree of f with edges E is equivalent to the max-tree of f with the set of edges $E''' = \cup E'''_k$ where:*

$$E'''_k = \begin{cases} \emptyset & \text{if } \min(f(u_{k-1}, f(v_{k-1})) < \min(f(u_k), f(v_k)) \\ \emptyset & \text{if } \min(f(u_{k+1}, f(v_{k+1})) < \min(f(u_k), f(v_k)) \\ E_k & \text{otherwise} \end{cases}$$

In figure 9c, we illustrate the grid simplification of the fully connected grid depicted in figure 9a and show that they lead to the exact same max-trees. The dashed edges for 8-connected simplified grid represent the edges removed from E' to E'' .

5.3 High dynamic range (HDR) images

As it stands, nothing prevents the current algorithm from running on high-quantized data. However, as described in [34], CONNECT is not efficient for those data as its

Configuration	Device	Model
Embedded	CPU	Jetson TX1 - 4 ARM Cortex-A57 @ 1.9Ghz
Embedded	GPU	Jetson TX1 - 256 Maxwell Cores @ 1.3Ghz
Desktop 1	CPU	2 i7-7567U cores @ 3.50Ghz
Desktop 1	GPU	GeForce GTX 1650 - 896 Cores @ 1.5Ghz
Desktop 2	CPU	6 i7-9750H cores @ 2.60Ghz
Desktop 2	GPU	GeForce RTX 2060 - 2176 Cores @ 1.4Ghz
Compute 1	CPU	20 Xeon Silver 4210 cores @ 2.20Ghz
Compute 1	GPU	Quadro RTX 8000 - 4608 cores @ 1.4Ghz
Compute 2	CPU	16 Xeon Silver 4110 cores @ 2.10Ghz
Compute 2	GPU	Tesla V100 - 5120 cores @ 1.3Ghz

TABLE 1: Hardware devices in the benchmark setup.

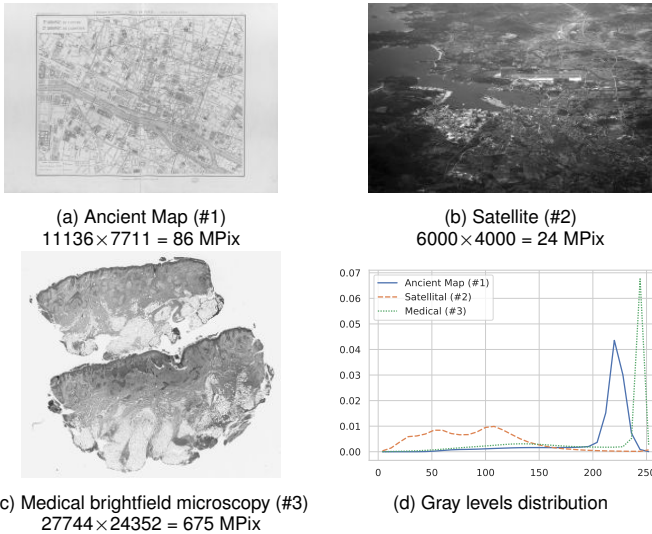


Fig. 11: The dataset used for benchmarking and the gray-level distribution of these images.

performance depends on the length of the branch (that drastically increases with the number of grayscale levels). In [29], the authors suggest duplicating the tile boundaries (called *halo*, see figure 10) so that CONNECT is called in global memory on two nodes with the same levels. The CONNECT procedure could be seen as two stages. The first step consists in traversing the chain to reach the nodes to merge, while the second step consists in merging the linked-lists of nodes. The *halo* technique enables us to reduce the amount of work done by the first step.

6 PERFORMANCE EVALUATION

6.1 Base benchmark

We compare the performance of our GPU implementation to the State-of-the-Art CPU ones. For the CPU part, the sequential Salembier’s algorithm (*Salembier ST*) implemented without recursion and pre-allocated priority queues are used. The parallel version (*Salembier MT*) uses a divide-and-conquer strategy. It runs Salembier’s algorithm on tiles and merges the trees hierarchically as described in [34]. The two GPU versions are the algorithm described in section 4 (*Base*) and its 1D-optimization from section 5.1 (*Optim 1D*). They are benchmarked with and without the memory transfer from and to the host memory. We have benchmarked on three profiles: embedded systems, desktop computers, and compute servers. Their descriptions are shown in table 1.

#	Algorithm	Local trees	Merge Global	Flatten	Total time
1	Base	88.7 (49%)	71.7 (40%)	19.8 (11%)	180.2
1	Optim 1D	45.3 (33%)	- (52%)	- (15%)	136.9
2	Base	23.0 (61%)	9.4 (25%)	5.3 (14%)	37.8
2	Optim 1D	11.7 (44%)	- (36%)	- (20%)	26.5
3	Base	646.9 (50%)	521.9 (40%)	120.4 (9%)	1289.2
3	Optim 1D	358.5 (36%)	- (52%)	- (12%)	1000.3

TABLE 2: Processing time (in milliseconds) of each kernel with the *Desktop 1* configuration on test images.

The benchmark also includes several image types shown in figure 11 (satellite images, medical images, and documents) to consider the variability of real image contents.

As one can see on figure 12, our GPUs versions outperform the sequential and the parallel version running on CPUs on comparable devices by at least a factor 5 on a single image. However, when processing a stream of images, the transfer latency from the host memory can be hidden and only the GPU kernel time has to be taken. Then, performance of *1D Optimized* is one order of magnitude higher than those on CPU.

When comparing the GPU algorithms, the 1D-optimization improves the performance by about 30% on average. Table 2 shows the kernel time distribution for the base algorithm and for the local max-tree optimized version. As one can see, the relative time spent by kernels depends on the image content, but the latter does not change the overall “kernel ordering”. Also, while the timings are for the *Desktop 1* configuration, the time distribution on the other architectures varies by $\pm 10\%$, but this is still representative to all test configurations. As depicted in table 2, the local max-trees computation time that represents more than half the GPU compute time is reduced by 50%. Several factors may explain this performance gain. First, the work per thread is much higher, because a single thread processes a full column (16x higher, because the columns are 16 pixels high). While it reduces the theoretical occupancy of the Streaming Multiprocessor (SM) and the number of active warps per SM, it actually leads to less contention between threads, because it reduces the number of concurrent *atomic writes* trying to update the same parent. From our experiment, the stall of individual warps (mostly due to atomics) and the thread divergence (mostly due to the FIND-PEAK-ROOT loop) are reduced by 25%.

It is worth mentioning that to speed up column merging and flattening of our *1D-optimized*, another work organization was tried. We tried running one thread per pixel, only using one thread per column during the 1D-construction part (yielding many idle threads) and then, using all the threads for column merging and flattening (more parallel work). However, this approach reduced the performance and showed that augmenting the work-per-thread to decrease the contention when merging was better.

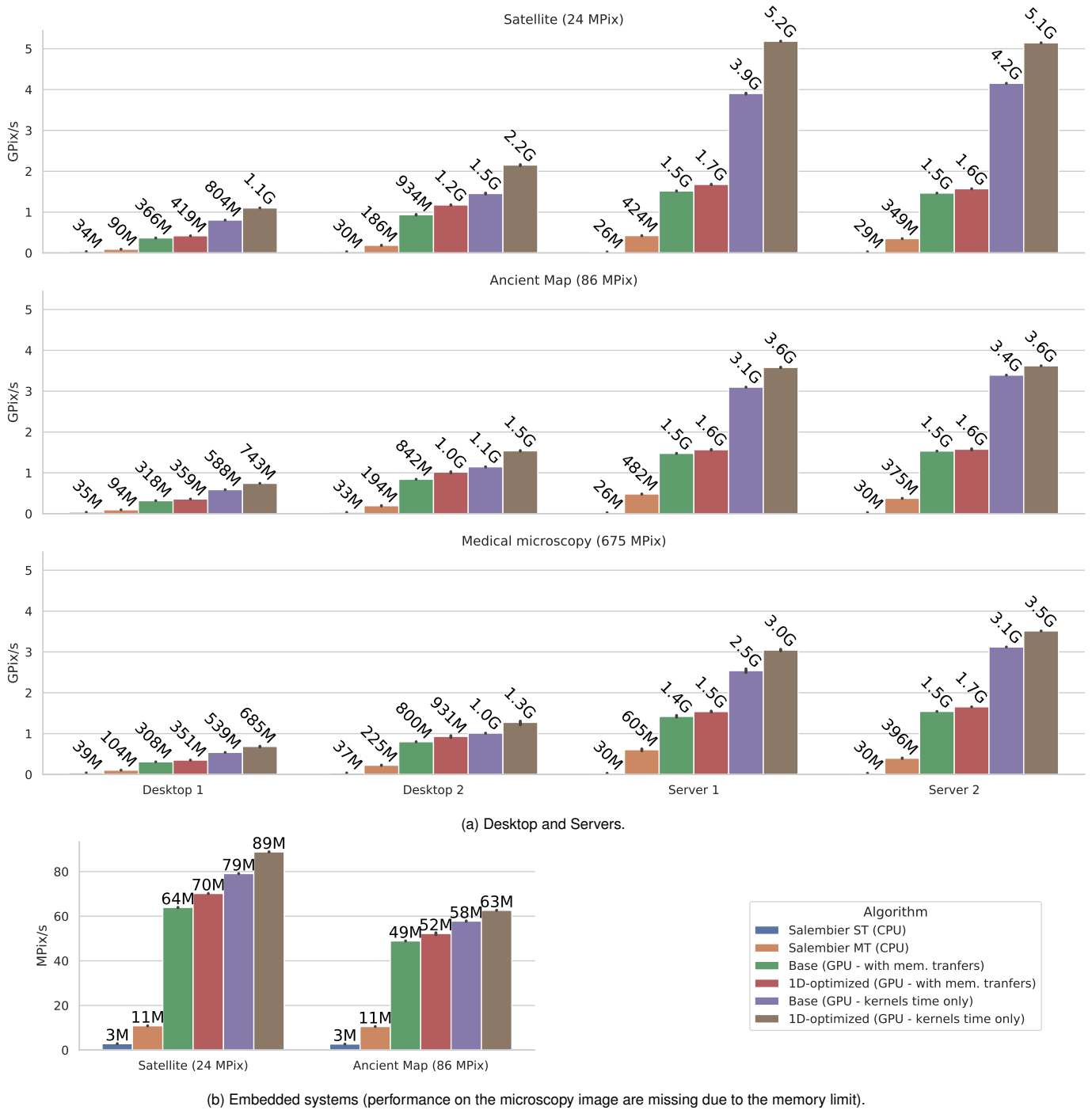


Fig. 12: Performance comparison of the max-tree computation with CPUs and GPUs on many hardware configurations and various image types. Benchmarks have been run 10 times and error bars represent the standard deviation of the measures.

6.2 Impact of the 8-connected grid

Figure 13 shows the impact of the 8-connectivity on the processing time. The processing time of the *base* algorithm increases by 120% on average, while the time of the *1D-optimized* algorithm is multiplied by a factor 2.5. Indeed, we have twice as many edges for the local max-tree computation but three times as many edges in the *global max-tree merging* step. Figure 13 also shows the effect of the grid simplification on the performance. In particular, the grid simplification for the 8-connectivity is always beneficial,

and we get back to the same running times as with the 4-connectivity baselines. With a 4-connected neighborhood, the grid simplification benefits are less obvious. This exhibits an interesting trade-off to have between “*more work, more contention but better work balancing and better parallelism*” and “*less work but unbalanced work and less parallelism opportunity*”. Indeed, in the extreme case where all boundary edges are replaced by a single link, a single thread has to merge the whole branch while the other threads are idle. The level of work done in parallel eventually drops while the branch could have been merged by several threads concurrently.

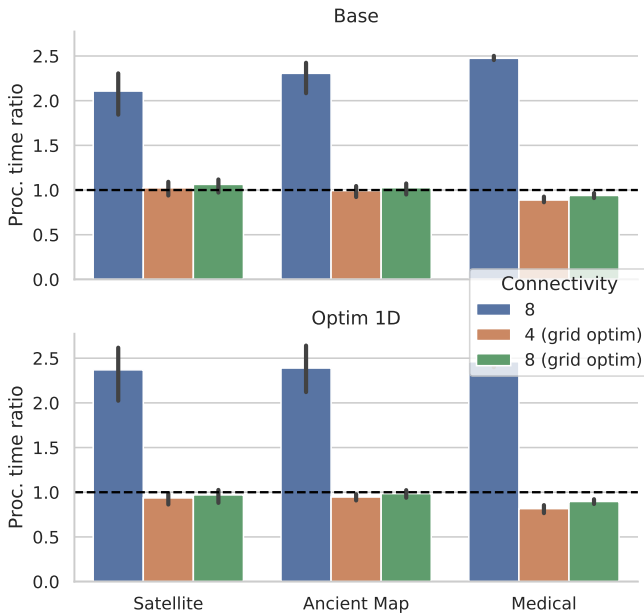


Fig. 13: Impact of the 8-connected neighborhood and the optimized connectivity grid. The processing time of the 4-connectivity kernels is used as a baseline. The processing time of each variant is expressed as a factor of the baseline time and averaged over the hardware configurations from table 1 (lower is better).

Image	Base (8b)	Base (16b)	Halo (16b)
#1	804 MPix/s	29.7 MPix/s	47.9 MPix/s
#2	588 MPix/s	18.4 MPix/s	29.6 MPix/s
#3	539 MPix/s	15.7 MPix/s	26.7 MPix/s

TABLE 3: Desktop 1 performance on 16-bit HDR test images compared to 8-bit images.

6.3 Impact of the HDR

To figure out the performance penalty of the quantization on our algorithm, we have transformed the original 24-bit RGB test images into 16-bit images. Following the protocol in [46], the luminance of RGB values is computed by $0.2126R + 0.7152G + 0.0722B$, and the value is quantized on 16 bits. In table 3, the second column shows the performance of our *Base* algorithm on 16-bit images and highlights a drastic slow-down (about 30 times slower). Actually, this slow-down is mostly due to the merge of max-trees in global memory that takes 90% of the total compute time. Indeed, with 16-bit images, there are more (canonical) nodes and the chain are longer. It follows that we hit the global memory at more random location (the L2 cache hit rate

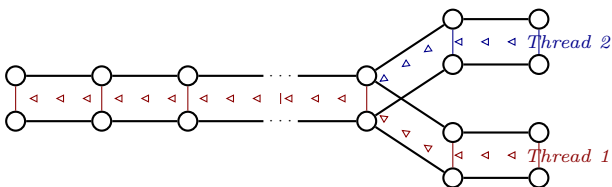


Fig. 14: Unbalanced merge work between threads. If two threads of the same warp merge two trees but have a low common ancestor, one thread is stalled and waits for the other to finish.

is less than 40%) and the memory latency is the leading cause of the thread stalls. Longer chains also induce less workload balancing between threads. Indeed, suppose that threads have to merge branches from two disjoint trees, but the branches meet soon in the hierarchy. One thread is going to be elected to merge the whole chain, while the others are being stalled waiting for the elected thread to finish. This problem is illustrated on figure 14. This thread divergence causes a low number of active threads per warp (less than 3 active thread/warp on some images).

With the *halo* technique, the cost of the first FIND-PEAK-ROOT in global memory is lower and compensates the extra-work induced to process the halo as shown in the third column of table 3 (adding and removing the halo counts only for 2% of the total time). Even if it improves slightly the performance, processing 16-bit images is still much slower than 8-bit images (up to 20 times slower).

Some interesting approaches have been proposed in [46], where the max-tree construction is “stratified” by buckets. An extension of our algorithm for high-dynamic images could probably benefit from these ideas, running the max-tree construction at different low-quantized bucket and eventually, merging them.

7 FUTURE WORK

3D images. The presented algorithm can easily be extended to 3D images. The max-tree algorithm depicted in section 5.1 could build the max-trees of the 2D slices. Then, the max-trees of the slices would be merged depth-wise just like we did for merging the 2D tiles vertically and horizontally. However, adding those *z*-connections would drastically reduce performance. Indeed, the maximal 26-connectivity would lead to a large amount of CONNECT issued in global memory during global max-tree merging. Even if the grid simplification trick could probably be extended in 3D, managing such a high amount of connection in global memory remains challenging.

Tree of Shapes (ToS) and Alpha-tree. As depicted in [22] the ToS can be computed using a max-tree algorithm. As stated, this approach benefits from efficient component-tree implementation. The newly presented max-tree GPU algorithm could serve as a foundation for efficient ToS computation. However, the method from [22] requires that we first transform the input images with 3 steps, namely *interpolation*, *immersion* and *propagation*. The first two steps can be trivially parallelized on GPU. Nevertheless, porting the *propagation* (that as the name suggests, uses a propagation flow) remains challenging on GPU.

Our algorithm seems to be also adapted to computing the α -Tree (*a.k.a.* the quasi-flat zone hierarchy). In this representation, the flat-zones are the leaves of the tree while the internal nodes are the edges of minimum spanning tree (MST) ordered by altitude. The most common α -tree algorithm [47], [48] is based on Kruskal’s MST algorithm and relies on the Union-Find. In [49], it has been observed that the α -tree is closely related to computing the min-tree on the *edge graph* of an image, and as a consequence, the adaptation looks straightforward.

8 CONCLUSION

In this work, the first massively parallel GPU algorithm for the computation of the max-tree has been presented. By taking advantages of the non-ending growth of the GPU computing performance, our algorithm is at least 5 times faster than the current State-of-the-Art CPU parallel algorithm and one order of magnitude faster when the memory transfer latency can be hidden. Moreover, we have proposed algorithmic variants that handle the 8-connectivity with no overhead and no added complexity. This work will especially benefit the recent researches dedicated to a distributed max-tree computation for terabyte images where each cluster node could compute a local max-tree of some subsection of data with the advantages of our GPU algorithm. Then, max-trees could be combined with some wider distributed algorithm. Finally, not only does this new algorithm enable the integration of the max-tree computation in GPU pipelines, but it also paves the way to port to GPUs many max-tree related structures as the Tree of Shapes.

As a matter of reproducible research, the source code of the GPU max-tree algorithm is available at <https://gitlab.lrde.epita.fr/nblin/max-tree>.

ACKNOWLEDGMENTS

The authors would like to thank Arthur Hennequin from LIP6 and LPNHE for having run our code on a V100 GPU. We would also like to thank Ilan Guenet from EPITA for helping on the performance tuning, as well as Alexandre Bourquelot and Reda Dehak from EPITA for the TX1 technical support. Image credits:

- Aerial view of Olbia - https://upload.wikimedia.org/wikipedia/commons/8/82/Aerial_view_of_Olbia.jpg
- Ancient Map - Atlases of Paris - Atlas municipal des vingt arrondissements de Paris. 1925. Bibliothèque de l'Hôtel de Ville. City of Paris. France. <https://bibliotheques-specialisees.paris.fr/ark:/73873/pf0000935524.locale=fr>
- Brightfield Microscopy (APERIO CMU-2.SVS) - <https://openslide.cs.cmu.edu/>

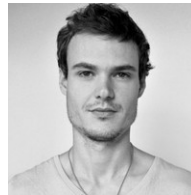
REFERENCES

- [1] M. Ôn Vù Ngoc, N. Boutry, J. Fabrizio, and T. Géraud, "A new minimum barrier distance for multivariate images with applications to salient object detection, shortest path finding, and segmentation," *Computer Vision and Image Understanding*, vol. 197–198, Aug. 2020.
- [2] P. Salembier, A. Oliveras, and L. Garrido, "Antiextensive connected operators for image and sequence processing," *IEEE Transactions on Image Processing*, vol. 7, no. 4, pp. 555–570, 1998.
- [3] L. Vincent, "Morphological grayscale reconstruction in image analysis: applications and efficient algorithms," *IEEE Transactions on Image Processing*, vol. 2, no. 2, pp. 176–201, 1993.
- [4] P. Salembier and J. Serra, "Flat zones filtering, connected operators and filters by reconstruction," *IEEE Transactions on Image Processing*, vol. 3, no. 8, pp. 1153–1160, 1995.
- [5] Y. Xu, T. Géraud, É. Puybareau, I. Bloch, and J. Chazalon, "White matter hyperintensities segmentation in a few seconds using fully convolutional network and transfer learning," in *International MICCAI Brainlesion Workshop*. Springer, 2017, pp. 501–514.
- [6] E. Puybareau and T. Géraud, "Real-time document detection in smartphone videos," in *Proceedings of the 25th IEEE International Conference on Image Processing (ICIP)*. IEEE, 2018, pp. 1498–1502.
- [7] R. Jones, "Component trees for image filtering and segmentation," in *IEEE Workshop on Nonlinear Signal and Image Processing*. Mackinac Island: E. Coyle, Ed., Sep. 1997.
- [8] —, "Connected filtering and segmentation using component trees," *Computer Vision and Image Understanding*, vol. 75, no. 3, pp. 215–228, 1999.
- [9] J. Hernández and B. Marcotegui, "Shape ultimate attribute opening," *Image and Vision Computing*, vol. 29, no. 8, pp. 533–545, 2011.
- [10] E. R. Urbach and M. H. Wilkinson, "Shape-only granulometries and grey-scale shape filters," in *Proceedings of the International Symposium on Mathematical Morphology (ISMM)*, vol. 2002, 2002, pp. 305–314.
- [11] G. K. Ouzounis and M. H. Wilkinson, "Mask-based second-generation connectivity and attribute filters," *IEEE Transactions on Pattern Analysis and Machine Intelligence*, vol. 29, no. 6, pp. 990–1004, 2007.
- [12] M. Dalla Mura, J. A. Benediktsson, B. Waske, and L. Bruzzone, "Morphological attribute profiles for the analysis of very high resolution images," *IEEE Transactions on Geoscience and Remote Sensing*, vol. 48, no. 10, pp. 3747–3762, 2010.
- [13] M. Dalla Mura, J. Atli Benediktsson, B. Waske, and L. Bruzzone, "Extended profiles with morphological attribute filters for the analysis of hyperspectral data," *International Journal of Remote Sensing*, vol. 31, no. 22, pp. 5975–5991, 2010.
- [14] G. K. Ouzounis, M. Pesaresi, and P. Soille, "Differential area profiles: Decomposition properties and efficient computation," *IEEE Transactions on Pattern Analysis and Machine Intelligence*, vol. 34, no. 8, pp. 1533–1548, 2011.
- [15] P. Bosilj, M. H. Wilkinson, E. Kijak, and S. Lefèvre, "Local 2d pattern spectra as connected region descriptors," *Mathematical Morphology Theory and Applications*, vol. 1, no. 1, 2016.
- [16] B. Mirmahboub, J. Moré, D. Youssefi, A. Giros, F. Merciol, and S. Lefèvre, "Fast pattern spectra using tree representation of the image for patch retrieval," in *International Conference on Discrete Geometry and Mathematical Morphology*, 2021, pp. 107–119.
- [17] J. Matas, O. Chum, M. Urban, and T. Pajdla, "Robust wide-baseline stereo from maximally stable extremal regions," *Image and Vision Computing*, vol. 22, no. 10, pp. 761–767, 2004.
- [18] D. Nistér and H. Stewénius, "Linear time maximally stable extremal regions," in *Proceedings of the 10th European Conference on Computer Vision (ECCV)*. Springer, 2008, pp. 183–196.
- [19] Y. Xu, T. Géraud, and L. Najman, "Connected filtering on tree-based shape-spaces," *IEEE Transactions on Pattern Analysis and Machine Intelligence*, vol. 38, no. 6, pp. 1126–1140, 2015.
- [20] M. A. Westenberg, J. B. T. M. Roerdink, and M. H. F. Wilkinson, "Volumetric attribute filtering and interactive visualization using the max-tree representation," *IEEE Transactions on Image Processing*, vol. 16, no. 12, pp. 2943–2952, 2007.
- [21] P. Monasse and F. Guichard, "Fast computation of a contrast-invariant image representation," *IEEE Transactions on Image Processing*, vol. 9, no. 5, pp. 860–872, 2000.
- [22] E. Carlinet, S. Crozet, and T. Géraud, "The tree of shapes turned into a max-tree: a simple and efficient linear algorithm," in *Proceedings of the 25th International Conference on Image Processing (ICIP)*. IEEE, 2018, pp. 1488–1492.
- [23] R. Souza, L. Tavares, L. Rittner, and R. Lotufo, "An overview of max-tree principles, algorithms and applications," in *Proceedings of the 29th SIBGRAPI Conference on Graphics, Patterns and Images Tutorials (SIBGRAPI-T)*. IEEE, 2016, pp. 15–23.
- [24] L. Najman and M. Couprie, "Building the component tree in quasi-linear time," *IEEE Transactions on Image Processing*, vol. 15, no. 11, pp. 3531–3539, 2006.
- [25] C. Berger, T. Géraud, R. Levillain, N. Widynski, A. Baillard, and E. Bertin, "Effective component tree computation with application to pattern recognition in astronomical imaging," in *Proceedings of the 18th International Conference of Image Processing (ICIP)*, vol. 4, San Antonio, TX, USA, Sep. 2007, pp. 41–44.
- [26] G. K. Ouzounis and M. H. Wilkinson, "A parallel implementation of the dual-input max-tree algorithm for attribute filtering," in *Proceedings of the International Symposium on Mathematical Morphology (ISMM)*, vol. 1, Oct. 2007, pp. 449–460.
- [27] M. Wilkinson, Hui Gao, W. Hesselink, J.-E. Jonker, and A. Meijster, "Concurrent computation of attribute filters on shared memory parallel machines," *IEEE Transactions on Pattern Analysis and Machine Intelligence*, vol. 30, no. 10, pp. 1800–1813, Oct. 2008.
- [28] P. Matas, E. Dokládlová, M. Akil, T. Grandpierre, L. Najman, M. Poupá, and V. Georgiev, "Parallel algorithm for concurrent computation of connected component tree," in *Advanced Concepts for Intelligent Vision Systems*, vol. 5259, 2008, pp. 230–241.

- [29] M. Gotz, G. Cavallaro, T. Geraud, M. Book, and M. Riedel, "Parallel computation of component trees on distributed memory machines," *IEEE Transactions on Parallel and Distributed Systems*, vol. 29, no. 11, pp. 2582–2598, Nov. 2018.
- [30] S. Gazagnes and M. H. Wilkinson, "Distributed connected component filtering and analysis in 2d and 3d tera-scale data sets," *IEEE Transactions on Image Processing*, vol. 30, pp. 3664–3675, 2021.
- [31] R. E. Tarjan, "Efficiency of a good but not linear set union algorithm," *Journal of the ACM*, vol. 22, no. 2, pp. 215–225, 1975.
- [32] W. H. Hesselink, "Salembier's min-tree algorithm turned into breadth first search," *Information Processing Letters*, vol. 88, no. 5, pp. 225–229, 2003.
- [33] M. H. Wilkinson, "A fast component-tree algorithm for high dynamic-range images and second generation connectivity," in *Proceedings of the 18th International Conference of Image Processing (ICIP)*, 2011, pp. 1021–1024.
- [34] E. Carlinet and T. Géraud, "A comparative review of component tree computation algorithms," *IEEE Transactions on Image Processing*, vol. 23, no. 9, pp. 3885–3895, Sep. 2014.
- [35] D. Menotti, L. Najman, and A. de Albuquerque Araújo, "1D component tree in linear time and space and its application to gray-level image multithresholding," in *Proceedings of the International Symposium on Mathematical Morphology (ISMM)*, 2007, pp. 437–448.
- [36] J. J. Kazemier, G. K. Ouzounis, and M. H. F. Wilkinson, "Connected morphological attribute filters on distributed memory parallel machines," in *Proceedings of the International Symposium on Mathematical Morphology (ISMM)*, 2017, pp. 357–368.
- [37] S. Gazagnes and M. H. F. Wilkinson, "Distributed component forests in 2-D: Hierarchical image representations suitable for tera-scale images," *International Journal of Pattern Recognition and Artificial Intelligence*, vol. 33, no. 11, Oct. 2019.
- [38] K. A. Hawick, A. Leist, and D. P. Playne, "Parallel graph component labelling with gpus and cuda," *Parallel Computing*, vol. 36, no. 12, pp. 655–678, 2010.
- [39] R. J. Anderson and H. Woll, "Wait-free parallel algorithms for the union-find problem," in *Proceedings of the twenty-third annual ACM symposium on Theory of computing*, 1991, pp. 370–380.
- [40] S. V. Jayanti and R. E. Tarjan, "A randomized concurrent algorithm for disjoint set union," in *Proceedings of the 2016 ACM Symposium on Principles of Distributed Computing*, 2016, pp. 75–82.
- [41] Y. Komura, "GPU-based cluster-labeling algorithm without the use of conventional iteration: Application to the swendsen-wang multi-cluster spin flip algorithm," *Computer Physics Communications*, vol. 194, pp. 54–58, 2015.
- [42] D. P. Playne and K. Hawick, "A new algorithm for parallel connected-component labelling on GPUs," *IEEE Transactions on Parallel and Distributed Systems*, vol. 29, no. 6, pp. 1217–1230, 2018.
- [43] A. Hennequin, L. Lacassagne, L. Cabaret, and Q. Meunier, "A new direct connected component labeling and analysis algorithms for GPUs," in *Proceedings of the Conference on Design and Architectures for Signal and Image Processing (DASIP)*. IEEE, 2018, pp. 76–81.
- [44] S. Allegretti, F. Bolelli, and C. Grana, "Optimized block-based algorithms to label connected components on GPUs," *IEEE Transactions on Parallel and Distributed Systems*, vol. 31, no. 2, pp. 423–438, 2019.
- [45] F. Lemaitre, A. Hennequin, and L. Lacassagne, "Taming voting algorithms on GPUs for an efficient connected component analysis algorithm," in *Proceedings of the International Conference on Acoustics, Speech and Signal Processing (ICASSP)*, 2021, pp. 7903–7907.
- [46] U. Moschini, A. Meijster, and M. H. Wilkinson, "A hybrid shared-memory parallel max-tree algorithm for extreme dynamic-range images," *IEEE Transactions on Pattern Analysis and Machine Intelligence*, vol. 40, no. 3, pp. 513–526, 2017.
- [47] G. K. Ouzounis and P. Soille, "The alpha-tree algorithm," *JRC Scientific and Policy Report*, 2012.
- [48] L. Najman, J. Cousty, and B. Perret, "Playing with kruskal: algorithms for morphological trees in edge-weighted graphs," in *Proceedings of the International Symposium on Mathematical Morphology (ISMM)*. Springer, 2013, pp. 135–146.
- [49] P. Soille and L. Najman, "On morphological hierarchical representations for image processing and spatial data clustering," in *Proceedings of the International Symposium on Mathematical Morphology (ISMM)*. Springer, 2010, pp. 43–67.



Nicolas Blin is currently pursuing an Ing. degree in image-processing at EPITA, Paris, France, and will graduate in 2022. He is also working as a research assistant at EPITA Research and Development Laboratory (LRDE). His research interests involve algorithms parallelization on GPU, mathematical morphology, and metaheuristic algorithms.



Edwin Carlinet received the Ing. degree from EPITA (Paris, France) in 2011, the M.Sc degree in Mathematics, Vision, and Machine Learning from ENS Cachan in 2012 and the Ph.D. degree in computer science from University Paris-Est in 2015. He is now an associate professor at EPITA. His research interests include HPC, in particular, the optimization of algorithms dedicated to Mathematical Morphology and Image processing. He is the maintainer of PYLENE <https://gitlab.lrde.epita.fr/olena/pylene>.



Florian Lemaitre Florian Lemaitre is a computer science postdoctoral researcher at Sorbonne Université. He works on the design and the optimization of new algorithms for micro-controllers, CPUs and GPUs. His expertise covers architectural code optimization, SIMD, multi-core, many-core, and GPU programming. He got an engineering degree in Computer Science at Ecole Supérieure d'Electricité (Supélec) in 2015 and a master degree in Computer Architecture at Université Paris-Sud. He received his doctorate in computer science from Sorbonne Université in 2019.



Lionel Lacassagne Lionel Lacassagne is a professor of computer science at Sorbonne University, formerly University Pierre et Marie Curie - Paris 6. His research focuses on the design of new algorithms for multi-core, many-core processors, and GPUs. He's working on high performance computing and image processing applied to embedded systems. He is an expert in code optimization for SIMD multi-core processors, GPUs, Cell processors, and VLIW DSP. Before his current post, he was an assistant professor at Paris-Sud University. He received his doctorate in robotics from Paris 6 University in 2000 and earned his engineering degree in computer science in 1995 at EPITA.



Thierry Géraud received the PhD degree in signal and image processing from Télécom Paris-Tech, in 1997, and the Habilitation à Diriger les Recherches from Université Paris-Est, in 2012. He is one of the main authors of the Olena platform, dedicated to image processing and available as free software under the GPL licence. His research interests include image processing, pattern recognition, software engineering, and object-oriented scientific computing. He is currently working with EPITA Research and Development Laboratory (LRDE), Paris, France. He is a member of the IEEE.